ChemPubSoc Europe

DOI: 10.1002/chem.201501675

CHEMISTRY
A European Journal
Full Paper

DNA Imaging

Serum Albumin Binding Inhibits Nuclear Uptake of Luminescent Metal-Complex-Based DNA Imaging Probes

Ashley Wragg,[a] Martin R. Gill,[b] Luke McKenzie,[a] Caroline Glover,[a] Rachel Mowll,[a] Julia A. Weinstein,[a] Xiaodi Su,[c] Carl Smythe,*[b] and Jim A. Thomas*[a]

Abstract: The DNA binding and cellular localization properties of a new luminescent heterobimetallic $Ir^{III}Ru^{II}$ tetrapyridophenazine complex are reported. Surprisingly, in standard cell media, in which its tetracationic, isostructural $Ru^{II}Ru^{II}$ analogue is localized in the nucleus, the new tricationic complex is poorly taken up by live cells and demonstrates no nuclear staining. Consequent cell-free studies reveal that the $Ir^{III}Ru^{II}$ complex binds bovine serum albumin, BSA, in Sudlow's Site I with a similar increase in emission and binding affinity to that observed with DNA. Contrastingly, in serum-free conditions the complex is rapidly internalized by live cells, where it localizes in cell nuclei and functions as a DNA imaging agent. The absence of serum proteins also greatly alters the cytotoxicity of the complex, where high levels of oncosis/necrosis are observed due to this enhanced uptake. This suggests that simply increasing the lipophilicity of a DNA imaging probe to enhance cellular uptake can be counterproductive as, due to increased binding to serum albumin protein, this strategy can actually disrupt nuclear targeting.

Introduction

The discovery that $[Ru(bpy)_2(dppz)]^{2+}$ (bpy = 2,2′-bipyridine, dppz = dipyridophenazine) binds DNA with a large increase in MLCT (metal-to-ligand charge transfer) emission[1] has generated great interest in luminescent d^6 octahedral transition metal complexes for biological applications.[2] These systems can reversibly bind DNA with high affinities and multiple binding modes.[3] While the majority of work has been in cell-free conditions, recently the cellular uptake and intracellular localization properties of these systems has been explored.[4]

Since these complexes have primarily been designed to bind DNA, efforts have been made to develop complexes that target genomic DNA within cell nuclei.[4,5] Consequently, it is somewhat surprising that examples of Ru^{II} systems capable of imaging nuclear DNA in live cells are still very limited. Despite this, we have found the dinuclear Ru^{II} complex $[(Ru(phen)_2)_2(tpphz)]^{4+}$ (phen = 1,10 phenanthroline, tpphz = tetrapyridophenazine), complex **1** (Scheme 1), is an effective live cell DNA imaging agent.[6] One drawback of this compound is that relatively high incubation concentrations (> 200 μM) are required to achieve satisfactory nuclear staining suitable for use with confocal laser scanning microscopy.

Strategies to improve cellular uptake of Ru^{II} DNA binding complexes include; increasing lipophilicity through, for example, the addition of hydrophobic ancillary ligands,[7] chemical linkage to targeting biomolecules,[8] organic dyes,[9] or nano-

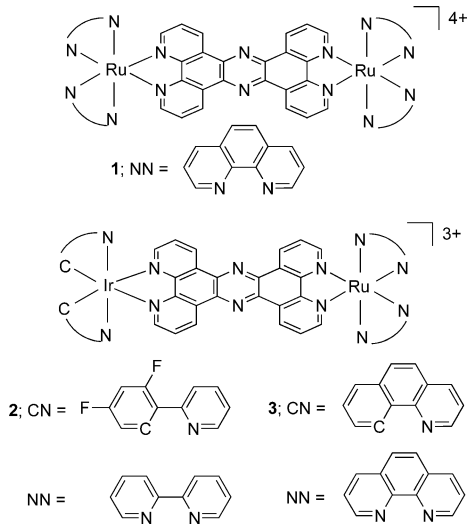

Scheme 1. Complexes relevant to this study.

[a] Dr. A. Wragg,[+] L. McKenzie, C. Glover, R. Mowll, Dr. J. A. Weinstein, Prof. J. A. Thomas
Department of Chemistry
University of Chemistry
Sheffield S3 7HF (UK)
Fax: (+44) 114-222-9346
E-mail: james.thomas@sheffield.ac.uk

[b] Dr. M. R. Gill,[+] Prof. C. Smythe
Department of Biomedical Science
University of Sheffield
Sheffield S10 2TN (UK)

[c] Dr. X. Su
Institute of Material Research and Engineering
A*STAR (Agency for Science, Technology and Research)
Singapore 117602

[+] These authors contributed equally to this work.

Supporting information for this article is available on the WWW under http://dx.doi.org/10.1002/chem.201501675.

particles[10] as well as general drug delivery strategies such as polymersome encapsulation.[11] However, while all these techniques promote *cellular* uptake, achieving consistent *nuclear* targeting evidently remains challenging. Clearly, this is a barrier in the development of such DNA binding systems towards live cell and, ultimately, in vivo applications.

One route to increased lipophilicity has been to prepare less cationic cyclometalated analogues of established systems; for example, a recent study on $[Ru(bpy)(phpy)(dppz)]^+$ (phpy = 2-phenylpyridine), a cyclometalated analogue of $[Ru(bpy)_2(dppz)]^{2+}$, showed that the resulting monocation rapidly targets the nuclei of cancer cells.[12] We have also investigated such effects: recently we demonstrated that the cell uptake properties of 4+ dinuclear Ru^{II} tpphz complexes are significantly improved in related heterobimetallic $Ir^{III}Ru^{II}$ tricationic cyclometalated systems, such as complex **2** (Scheme 1).[13]

In this work, we describe the imaging properties of a new bimetallic $Ir^{III}Ru^{II}$ complex $[(bhq)_2Ir(tpphz)Ru(phen)_2]^{3+}$ (bhq = benzo[*h*]quinolone), **3**, which is an isostructural tricationic analogue of the live cell DNA imaging agent **1** (Scheme 1). Surprisingly, biophysical and cell uptake properties of the new complex differ remarkably from those of **1**. Its properties provide evidence that decreasing the charge density of an imaging probe can be counterproductive and may lead to *decreased* cell uptake and nuclear localization due to strong binding with serum albumin protein.

Results and Discussion

Complex **3** was prepared by a reported method[13,14] and characterized by NMR, ESI-MS, and accurate mass and elemental analyses (full details are given in the Experimental Section and in Figures S1 and S2 in the Supporting Information). UV/Vis spectra of **3** in acetonitrile (as the PF_6^-salt) or water (as the Cl^-salt) show intense LC (ligand-centered) bands in the UV region (< 300 nm); tpphz bridging ligand absorption bands around 370 nm, and broad ^{1}MLCT absorptions, with maxima at 418 or 440 nm in acetonitrile or water respectively (see Figure S3). Complex **3** is emissive in both solvents, where excitation into the MLCT region results in emission with maxima at 604 nm (MeCN) or 616 nm (H_2O) (see Figure S4). As common for Ru^{II} polypyridyl complexes,[14] **3** demonstrates a reduced emission intensity in water compared to acetonitrile ($\phi = 2.2\times10^{-3}$ and 4.4×10^{-3} in H_2O and MeCN, respectively).

Whilst the distinctive emission of d^6 metal coordination complexes is useful for advanced microscopy techniques,[15] high energy excited states may generate $^1O_2$ or other ROS (reactive oxygen species), resulting in phototoxicity. While this is a significant drawback for imaging, it is useful for photodynamic therapy (PDT). Indeed, several monometallic cyclometalated Ir^{III} complexes have been investigated as cellular PDT photosensitizers.[16] Accordingly, the singlet oxygen quantum yield ($\phi\Delta$) of $[\mathbf{3}](PF_6)_3$ was measured in CH_2Cl_2 using perinaphthenone as the standard. In these conditions a low singlet oxygen quantum yield, $\phi\Delta$, of 0.0582 ± 0.002 was obtained, indicating that **3** is a poor $^1O_2$ sensitizer compared to reported PDT leads.[17] This is, of course, a distinct advantage for luminescent cell imaging. Not only are these observations consistent with the emission data, they agree with previous studies on related Ir^{III}–Ru^{II} systems showing that excitation leads to the lower energy Ru-centered excited state being occupied.[13]

Since both **1** and **2** show increased emission when bound to DNA,[6a,13,18] the luminescence of **3** in the presence of DNA was investigated. As indicated by Figure 1, the emission intensity of

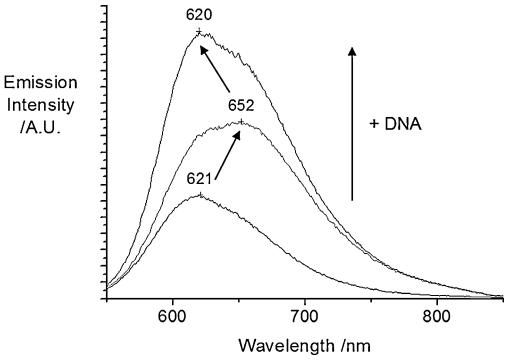

Figure 1. MLCT luminescence increase of **3** with addition of DNA in aqueous solution (5 mM Tris, 25 mM NaCl, pH 7.4). Note two-step binding with distinct maxima at 652 nm and 620 nm.

3 clearly increases on progressive addition of DNA. This well-established effect is the result of the greater emissive properties of **3** in hydrophobic environments combined with shielding of **3** from water upon DNA binding.[1,6a,18]

Uniquely, the emission increase of **3** upon DNA addition occurs in two steps: Initially, at low [DNA]/[**3**] ratios, emission increases are accompanied by red-shifting (621→652 nm), but at higher [DNA]/[**3**] ratios, the emission blue-shifts (652→620 nm) so that the final emission profile closely resembles the original spectra of **3** in water, albeit at a greater intensity. Isolation of these two binding phases from the emission data was accomplished by plotting the differences between emission points, and the consequently constructed curves are shown in Figure S5. Fitting the two individual phases to the McGhee–von Hippel model[19] produced an equilibrium binding constant, $K_b = 7.0\times10^6\,M^{-1}$ and site size, $S = 1.6$ for the first binding event and a lower affinity of $K_b = 2.2\times10^5\,M^{-1}$, but larger site size, $S = 2.7$, for the second event. Clearly, complex **3** appears to interact with DNA in a more complex manner to **1** or **2**.[6a,13] As the second phase occurs at high [DNA], this suggests that complex **3** is capable of crosslinking or condensing DNA—a possibility that is currently being investigated. Nevertheless, these studies demonstrate that **3** binds DNA with high affinity and a distinctive emission signature. Consequently, its ability to bind—and visualize—cellular DNA was investigated by confocal laser scanning microscopy, CLSM.

Initially, ethanol-fixed HeLa human cervical cancer cells were stained with the $Ir^{III}Ru^{II}$ complex and visualized by CLSM. These fixation conditions facilitate unimpeded access to the cell nucleus by removing the main barrier to cellular uptake: transport across the plasma membrane. As shown in Figure 2a, fixed HeLa cells stained with 10 μM **3** display intense nuclear

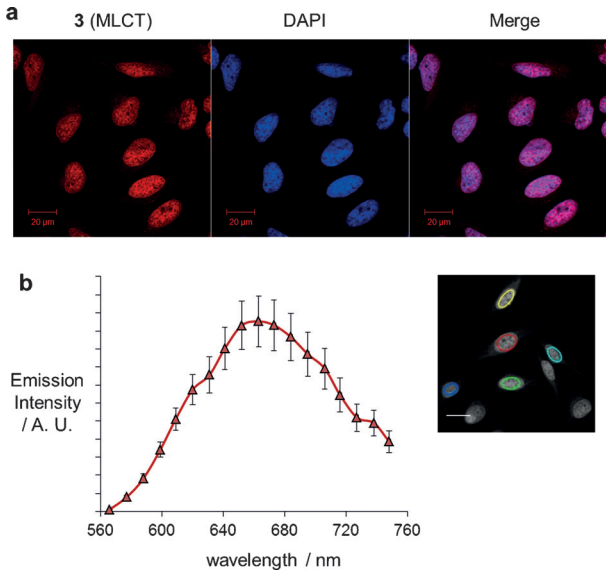

Figure 2. a) CLSM of ethanol-fixed HeLa cells co-stained with **3** (10 μM, 10 min) and DNA dye DAPI (500 nM, 5 min) showing overlap of signals (right-hand panel). MLCT: λ_{ex} = 488 nm, λ_{em} = 575–750 nm. DAPI: λ_{ex} = 405 nm, λ_{em} = 410-500 nm. b) Emission profile of chromatin-bound **3** in ethanol-fixed HeLa cells (λ_{ex} = 488 nm, λ_{em} = 560–760 nm). Data average of five nuclei stained ± S.D. (Inset, scale bar = 20 μm).

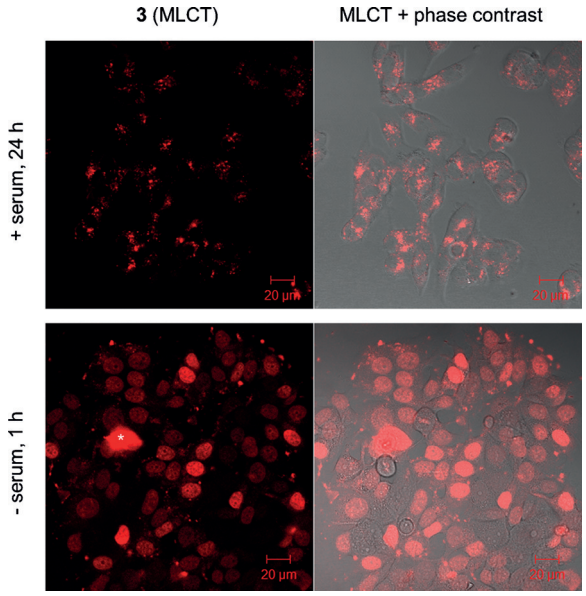

Figure 3. CLSM of live MCF7 cells incubated with 10 μM **3** in either 10% serum (24 h, top panels) or serum-free (1 h, bottom panels) media. MLCT and phase contrast (λ = 488 nm) + MLCT merged images included. *Indicates a necrotic (membrane-compromised) cell, as distinguished by the high emission intensity.

MLCT-based emission which strongly co-localizes with the well-established DNA dye DAPI (4′,6-diamidino-2-phenylindole). Examining the emission spectrum of nuclei stained by **3**, it is apparent that the dominant emission peak is centered at ~650 nm (Figure 2b). This corresponds to the primary, higher affinity, binding event observed in our cell-free DNA binding studies.

Strikingly the 620 nm emission is not observed. However, although nuclear DNA content is high, within cells it is packed into highly condensed chromatin. In contrast—in aqueous solution—unpacked, solvated DNA can interact with the complex in a more intimate binding geometry.

Having confirmed that **3** can bind to and visualize chromatin, we then explored its cellular uptake by live cells. First, the impact of **3** on cell proliferation was characterized by incubating MCF7 human breast cancer cells or HeLa cells with solutions of **3** (0.1–100 μM) for 24 h and resultant cell viability determined through MTT metabolic activity assay (MTT = 3-(4,5-dimethylthiazol-2-yl)-2,5-diphenyltetrazolium bromide). The previously reported complex **2** was included in parallel for comparative purposes. Both $Ir^{III}Ru^{II}$ complexes demonstrate a moderate impact on MCF7 cell metabolic activity, with comparable half inhibitory concentrations (IC_{50}s) of (27 ± 1) and (25 ± 1) μM for **2** and **3**, respectively (Figure S6); while a reduced potency towards HeLa cells is observed for **3** (IC_{50} = 47 μM, Figure S7).

To investigate the live cell uptake and localization of **3**, MCF7 cells were initially incubated with 10–30 μM **3** in standard cell medium and the resultant cellular uptake and intracellular localization assessed by CLSM. Somewhat surprisingly, incubation with 10 μM **3**, even for periods as long as 24 h, generally results in poor, non-specific intracellular emission and no nuclear staining (Figure 3, top panels, and Figure S8). The cytotoxicity of **3** prevented higher concentrations being utilized due to high levels of cell necrosis induced by the complex (Figure S8b). In the light of conventional wisdom, these results are surprising, as closely related studies[12] indicate that the lower charge density of the cyclometalated **3** would enhance uptake relative to the more cationic isostructural complex **1**. These results led us to consider whether complex **3** was now binding to other targets.

A likely candidate in live cell culture is serum albumin protein. Specific metal complexes have been shown to interact with serum albumin proteins as illustrated by the development of optical probes for human serum albumin (HSA).[20] It has also been suggested that interactions of a metal coordination complex with serum albumin, a protein found at millimolar levels within blood, may well impair the potency of both anticancer[21] and anti-bacterial[22] metal-based therapeutic candidates. In this context, we investigated interaction of **3** with bovine serum albumin (BSA), a structural homologue of HSA,[23] and a common component of cell culture media.

In cell-free conditions, addition of BSA to a solution of complex **3** results in an increase in luminescence of **3** (Figure 4a). However, in contrast to titrations with DNA, emission maxima remain at 615 nm. This suggests that **3**, or analogues, can be developed as optical probes for proteins, particularly serum albumin. Attempts to calculate binding affinities through a Scatchard analysis yielded nonlinear plots, suggesting that **3** binds to multiple sites within the BSA structure, thus a K_b value was not obtainable through this method. Considering **3** is a bulky, coordinately inert complex, we hypothesized that one such possible binding site could be Sudlow site I: a hydrophobic cavity and known binder of hydrophobic drugs.[24] Ac-

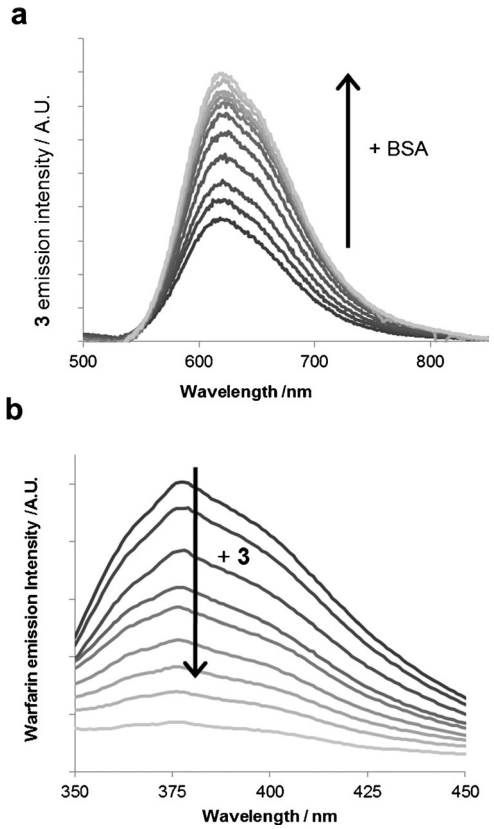

Figure 4. a) MLCT luminescence increase of **3** with addition of BSA (5 mM Tris, 25 mM NaCl, pH 7.4). b) Decrease in Warfarin fluorescence upon addition of **3** to Warfarin:BSA (2:1) mixture (5 mM Tris, 25 mM NaCl, pH 7.4).

cordingly, a competition assay with **3** and the Sudlow site I-specific ligand Warfarin[25] was undertaken. As Warfarin ($K_b = 4.8\times10^5\ M^{-1}$) demonstrates a 10-fold increase in fluorescence emission when localized within Sudlow site I,[26] we elected to employ a competition binding assay and measure the change in Warfarin fluorescence intensity to determine the fraction of Warfarin bound as a function of concentration of **3**. As shown in Figure 4b, the addition of **3** to a 2:1 BSA:Warfarin solution results in a decrease in Warfarin fluorescence where, at a high [complex]:[Warfarin] ratio, the relative emission intensity is reduced to 10%.

These results confirm that **3** binds this specific site in BSA. Applying an equilibrium ligand binding model, these data facilitate determination of a dissociation constant, $K_d = 23\ \mu M$, which corresponds to a $K_b(BSA) = 4.5\times10^4\ M^{-1}$. While this binding affinity is lower than that observed for **3** with DNA, it is comparable to values obtained for structurally related hydrophobic mononuclear Ru^{II} compounds,[27] and is greater than the BSA affinity of the DNA groove-binder DAPI ($K_b = 1\times10^4\ M^{-1}$).[28] However, given the results of the Scatchard analysis, it seems likely that **3** may very well interact with other sites within BSA.

Having verified that complex **3** binds bovine serum albumin with a relatively high affinity, we investigated its cellular uptake in serum-free conditions. In complete contrast to our initial studies, MCF7 cells incubated with 10 μM **3** in serum-free medium for only 60 min now efficiently internalize the complex and the nuclei of cells are clearly visualized by the complex (Figure 3, bottom panels). Strikingly, effective imaging using **3** requires an incubation concentration fiftyfold lower than the effectively isostructural dinuclear Ru^{II} analogous complex **1** (10 μM and 500 μM for **3** and **1**, respectively), in agreement with the principle that the lower charge of the cyclometalated complex has resulted in improved uptake.[12] Furthermore, **3** offers an improved rate of nuclear accumulation over the related $Ir^{III}Ru^{II}$ DNA imaging complex **2** (Figure S9), consistent with the notion that phen-based ancillary ligands promote cellular uptake over their bpy-analogous counterparts.[6b,7a,29]

The large serum-induced changes in uptake observed for **3** is not a general phenomenon: complex **1** retains nuclear staining in serum-containing media, whilst $[Ru(bpy)_2(dppz)]^{2+}$, the original light switch complex,[1] still fails to stain nuclei even in serum-free conditions (see Figure S10 and S11). However, for **3** this effect is not just restricted to MCF7 cells; in HeLa cells it is even more pronounced: cells incubated with 20 μM **3** clearly show high levels of emission from the cell nucleus when incubated in serum-free media, compared to negligible MLCT emission from cells incubated in serum-containing media (Figure 5a and S12).

While the relationship between cellular uptake and cell viability for inert metal complexes is typically compared within a series of closely related complexes,[4,5] the results for **3** provide an opportunity to *isolate* the effect of cellular/nuclear uptake of **3** on bioactive potency. We therefore explored the impact of these radically different levels of cellular uptake upon cell viability. To achieve this, HeLa cervical cancer cells were first treated with solutions of **3** in either serum-containing or serum-free media for 80 min, the solutions were then removed and replaced with fresh, complex-free (and serum-containing) media, then relative cell viabilities were measured 48 h later by MTT assay. Respective blanks for each condition were defined as having a relative cell viability of 100%. The results showed that, in HeLa cells, pre-treatment with 10 or 20 μM **3** in serum-free media strongly affects cell proliferation, as cell viabilities of 53% and 17% were obtained for these respective conditions (Figure 5b). Significantly, HeLa cells pre-treated with the same concentrations of **3** but in serum-containing media retain ~100% relative cell viability. These results clearly indicate that the cellular uptake of **3**, as promoted by serum-free incubation conditions, leads to a significant impact on cell viability, which is confirmed as cytotoxicity by inspection. When cellular uptake is blocked by serum binding no impact on metabolic activity is observable.

Examining the mode of induced cell death, minimal levels of the apoptotic marker cleaved caspase-3[30] are observed in HeLa cells treated with **3** (Figure 5c, middle panels), indicating low levels of apoptosis within **3**-treated cell populations. Furthermore, no generation of a proxy marker of DNA double-strand breaks, phospho-histone H2AX (γ-H2AX),[31] is observed above an untreated control (Figure 5c, top panels). Both these findings are in stark contrast to cells treated with the DNA cross-linking agent cisplatin which, as expected,[32] induces high levels of both cleaved caspase 3 and γ-H2AX (Figure 5c).

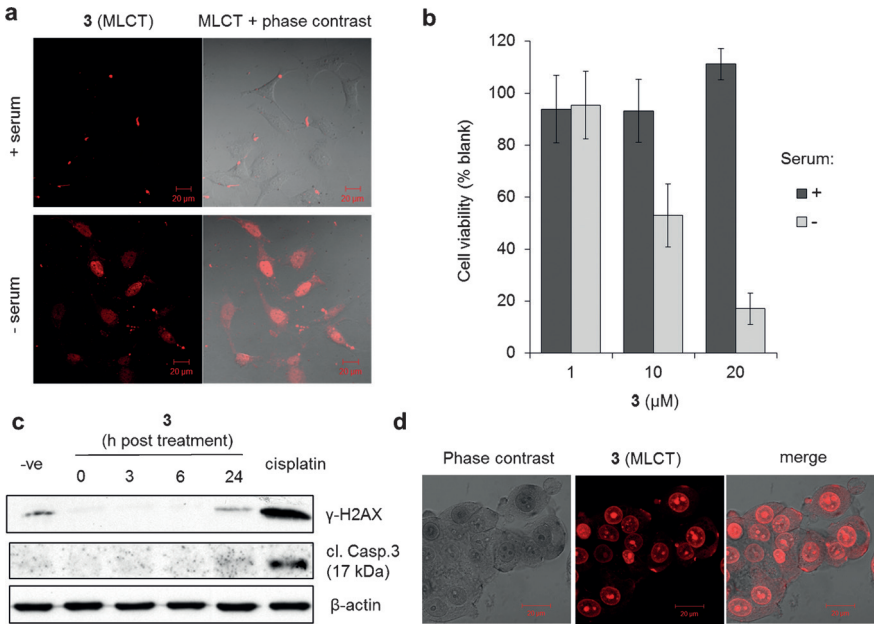

Figure 5. a) CLSM of HeLa cells incubated with **3** (20 μM, 80 min) in either 10% serum (top panels) or serum-free (bottom panels) media. MLCT (left) and MLCT + phase contrast (right) micrographs shown. Identical MLCT microscopy parameters used. b) Resultant cell viability of HeLa cells pre-treated with 1, 10 or 20 μM **3** (80 min) in either 10% serum or serum-free media. Metabolic activity measured 48 h after treatment by MTT assay. Data average of two independent experiments ± S.D. c) Levels of DNA damage (ds breaks) marker γ-H2AX and apoptotic marker cleaved caspase 3 (17 kDa fragment) in HeLa cells pre-treated with **3** (10 μM, 80 mins, serum-free media). Lysates prepared 0-24 h post-complex removal. Cisplatin (30 μM, 24 h) was used as a positive control. β-actin was employed as a loading control. d) Morphological evidence for secondary necrosis in **3**-treated HeLa cells (50 μM, 80 min, serum-free conditions), including cell swelling, debris, disintegration of plasma membrane and swollen (but intact) nuclei.

Instead, a clear oncotic/necrotic cellular morphology is observed for cells treated with cytotoxic doses of **3** (Figure 5d and Figure S13); a death response characterized by cell and nuclear swelling, membrane damage followed by eventual loss of plasma membrane integrity.[33] Taken together, these results indicate that **3** induces cell death primarily via an oncotic/necrotic mechanism and without generation of DNA damage (double strand breaks); a somewhat surprising result considering the high nuclear uptake of **3** in these conditions.

Nuclear staining by the previously reported and structurally related $Ir^{III}Ru^{II}$ complex **2** is also inhibited by serum proteins and serum-free treatment conditions deleteriously affect cell viability compared to cells treated equivalently in serum-containing media (Figure S14). Unlike the cellular responses induced by the two cyclometalated tricationic complexes, cell viability after treatment with **1** is relatively unaffected by either serum-containing or serum-free media; results consistent with comparable levels of nuclear staining in these different conditions, as described previously (see Figure S10).

While this study specifically examined the binding interaction of **3** with albumin, the major component of BSA used in cell culture, it should be noted that **3** may well bind other serum proteins. Work involving screening a variety of serum proteins for binding interactions with **3** would be highly revealing in this regard. Considering the attractive luminescent properties that accompany binding, **3**, and its derivatives, may find application within a serum protein imaging context; for example, assessing cellular uptake pathways of specific serum proteins in a relevant medical context.[34]

The observations outlined in his report have more general implications. A chemical strategy commonly employed to promote cellular uptake of DNA-binding metal complexes—particularly with a view towards improving nuclear accumulation—involves increasing hydrophobicity/decreasing charge with the overall aim of generating lipophilic complexes.[5] The results outlined in this report suggest that this approach may inadvertently generate high-affinity, serum protein-binding systems which will concomitantly have a negative impact on a probe's ability to successfully target cell nuclei. In a wider context, as luminescent complexes are developed towards in vivo applications, such factors may affect the ability of therapeutic leads and imaging agents to be internalised by cells and to subsequently localize at their intracellular target(s). This is of particular relevance for therapeutic and/or imaging candidates that would require clinical administration via blood.

Conclusion

In conclusion, in cell-free conditions, the new bimetallic $Ir^{III}Ru^{II}$ complex $[(bhq)_2Ir(tpphz)Ru(phen)_2]^{3+}$ binds DNA by reversible mechanisms with a distinctive "two step" increase in MLCT luminescence. Live cell uptake studies reveal the ability of the molecule to target—and successfully image—the nucleus of live cells is strongly inhibited by serum proteins; a finding we rationalize as being due to a high binding affinity for serum albumin.

Experimental Section

Syntheses: Complexes **1**, **2** and $[Ru(bpy)_2(dppz)]^{2+}$ were prepared as previously reported.[1,13,14] Synthesis of complex **3**: $[(phen)_2Ru(tpphz)]Cl_2$[14,29a] (200 mg, 0.218 mmol) was fully dissolved in 40 mL degassed ethanol. $[Ir(bhq)_2Cl]_2$[35] (175 mg, 0.149 mmol) was added and the solution heated to reflux for 12 h. After reflux, the solution was cooled to −10 °C and filtered to remove unreacted iridium dimer. A saturated solution of NH_4PF_6 (4 mL) in 100 mL of water was then added to precipitate the product. The precipitated complex was filtered and washed thoroughly with water to remove excess PF_6. Column chromatography on silica (eluent: CH_3CN/H_2O/aq. KNO_3, 100/5/2), followed by anion ex-

change using NH_4PF_6 to give the 142 mg of $\mathbf{3}(PF_6)_3$ (0.078 mmol) as an orange solid in a 36% yield. ^{1}H NMR (400 MHz, CD_3CN): $\delta =$ 10.07 (d, $J = 8.3$ Hz, 1H), 10.00–9.91 (m, 1H), 8.66 (d, $J = 8.3$ Hz, 2H), 8.52–8.47 (m, 1H), 8.44 (d, $J = 8.1$ Hz, 1H), 8.31 (t, $J = 2.6$ Hz, 2H), 8.30–8.24 (m, 2H), 8.09 (t, $J = 6.2$ Hz, 2H), 8.06–7.99 (m, 2H), 7.90 (dd, $J = 8.3$, 5.4 Hz, 1H), 7.86 (d, $J = 8.0$ Hz, 1H), 7.73–7.66 (m, 2H), 7.62 (t, $J = 10.4$ Hz, 1H), 7.42–7.34 (m, 1H), 7.29 (t, $J = 7.6$ Hz, 1H), 6.45 ppm (t, $J = 8.8$ Hz, 1H). ESI-MS: 1685 for $[\mathbf{3} + 2PF_6]^+$, 770 for $[\mathbf{3} + PF_6]^{2+}$, 465 for $[\mathbf{3}]^{3+}$. Accurate mass calcd for $C_{74}H_{44}N_{12}F_{12}P_2IrRu$: 1685.1768; found 1685.1696. Elemental analysis calcd (%) for $C_{74}H_{44}F_{18}IrN_{12}P_3Ru$: C 48.58, H 2.42, N 9.19; found: C 49.12, H 2.55, N 9.06.

Photophysical studies: Fluorescence measurements were made using a FluoroMax-4. Absorption spectra were recorded using an Agilent Technologies Cary 3000. Quantum yield determination was carried out as previously described[7c] using $Ru(bpy)_3^{2+}$ in acetonitrile ($\Phi = 0.062$)[36] as the reference. Singlet oxygen quantum yield ($\phi\Delta$) in dichloromethane was determined as previously described[37] employing 355 nm excitation and perinaphthenone as the standard ($\phi\Delta$ perinaphthenone = 95%).[37]

DNA binding studies: Calf thymus DNA (CT-DNA) was purchased from Sigma as a solid sodium salt and dissolved in buffer (5 mM Tris, 25 mM NaCl, pH 7.0). An average chain length of 150–200 base pairs (bp) was achieved by subjecting the CT-DNA solution to 30 min of discontinuous sonication using a Sanyo Soniprep 150 ultrasonic disintegrator, fitted with a 19 mm diameter probe. Purity of the sample was determined by UV/Vis spectroscopy, with $A_{260}/A_{280} > 1.9$ indicating a protein-free sample. DNA concentration was also determined by UV/Vis spectroscopy using 260 nm, $\varepsilon =$ 13,200 $M^{-1}cm^{-1}$ for concentration analysis. All solutions used in the DNA binding studies were dissolved in 5 mM Tris buffer. DNA solutions occurred by addition of DNA to known concentration of $\mathbf{3}(Cl)_3$ in Tris buffer. Emission of the complex was recorded, nonlinear Scatchard plots (r/Cf versus r) constructed and fitted by a McGhee–von Hippel model.[19]

BSA binding studies: BSA binding analysis occurred by addition of BSA (fraction V, Sigma) to a known concentration of $\mathbf{3}(Cl)_3$ in Tris buffer. Emission of the complex was recorded with increasing [BSA]/[$\mathbf{3}(Cl)_3$]. Warfarin competition binding assays were undertaken following a literature procedure[22b] with BSA used in place of HSA. For determination of the binding constant of **3** with BSA, the K_d (equilibrium dissociation constant) half inhibitory concentration was extrapolated from a Warfarin intensity/[**3**] log *C* plot (R^2 value = 0.9949), where $IC_{50} = K_d$ for an equilibrium binding model. The equilibrium binding constant, K_b, was calculated as the reciprocal of K_d.

Cell culture: MCF7 cells were cultured in RMPI1640 (Sigma) supplemented with 10% fetal bovine serum (FBS) and penicillin/streptomycin. HeLa human cervical cancer cells were cultured in DMEM (Sigma) supplemented with 10% FBS and penicillin/streptomycin. Cells were maintained at 37 °C in an atmosphere of 5% CO_2 and routinely sub-cultured using Trypsin.

Cell proliferation (MTT) assays: Cells were seeded in 48 well plates at a density of 20000 cells/well and allowed to proliferate for 24 h. Cells were treated as stated in the main text (in triplicate). Resultant cell viabilities after treatment were quantified using 0.5 mg mL^{-1} MTT (3-(4,5-dimethylthiazol-2-yl)-2,5-diphenyltetrazolium bromide) in serum-free media for 60 min. The formazan product was eluted using acidified isopropanol, absorbance at 540 nm quantified by spectrophotometer (reference = 640 nm), and cell viability determined as % of an untreated drug-free control for each experimental condition. Where appropriate, the corresponding half inhibitory IC_{50} concentration for the conditions was extrapolated from cell viability/log *C* plots. Serum-free versus serum experiments involved pre-treating cells with solutions of **3** before removal of the complex, washing with PBS, and replacement with fresh, complex-free (and serum-containing) media. Viability was measured 48 h after complex removal.

Confocal microscopy: For fixed cell imaging, cells were grown on glass coverslips, fixed using 70% ethanol and washed with PBS. Samples were stained with 10 μM **3** for 10 min and washed with PBS. Where appropriate, co-staining with DAPI (500 nM in PBS) for 5 min was performed after this step. For live cell imaging, cells were seeded in glass-bottomed Ibidi μ-dishes (Thistle Scientific) and allowed to proliferate for 24 h. After removal of growth media, cells were treated with solutions of the relevant complex (concentration/time as stated in main text) at 37 °C. After incubation, cells were washed with PBS and fresh media added before visualization. Samples were luminescently imaged on a Zeiss LSM 510 META inverted confocal laser microscope using 40x or 63x oil-immersion objectives. **3** and **2** were excited with an Ar-ion laser at 488 nm and emission collected with a 575 nm (red) LP (long pass) filter. Lambda stacking experiments (emission profiles) employed 488 nm excitation and the emission intensities collected at a range of 566–748 nm, at intervals of 11 nm. DAPI was excited using a 405 nm diode laser and emission detected using a 420–480 nm (blue) BP (band pass) filter. **1** was excited using 458 nm and the emission detected 670–700 nm. SYTO9 was excited at 488 nm and emission detected with a 500–530 nm BP filter. $[Ru(bpy)_2(dppz)]^{2+}$ was excited at 458 nm and emission detected 600–700 nm. Image data acquisition and processing was performed using Zeiss LSM Image Browser or MacBiophotonics ImageJ software.

Western blotting: HeLa cells were treated with 10 μM **3** for 80 m before the addition of fresh, non-complex (and serum-containing) media. At 0–24 h time points post-incubation cells were washed with cold PBS, detached using cell scraper and lysed in lysis buffer (20 mM Tris, pH 7.5, 0.27 M sucrose, 1 mM EDTA, 1 mM EGTA, 1% Triton X-100, protease inhibitors (10 μg mL^{-1} leupeptin, 2 μg mL^{-1} pepstatin, 50 μg mL^{-1} antipain, 2 μg mL^{-1} aprotinin, 20 μg mL^{-1} chyprostatin and 2 μg mL^{-1} benzamidine), and phosphatase inhibitors (50 mM NaF, 1 mM Na_3VO_4 and 20 mM β-glycerophosphate) via freeze/thawing cycles (x3). Protein content of lysates was quantified via Bradford assay. Aliquots of cell lysates were resolved by 12% SDS-PAGE (20 μg total protein/well), transferred onto nitrocellulose membrane and probed with antibodies that recognise the active (cleaved) form of caspase 3 (Cell Signaling, 1/1000 dilution) or γ-H2 AX (phospho-H2 AX (Ser139)) (Millipore, 1/1000). β-actin antibodies (Sigma, 1/5000) were employed to provide a loading control. Reactions were visualized with a suitable secondary antibody conjugated with horseradish peroxidase before ECL or ECL+ chemiluminescence reagents (GE Healthcare Life Sciences) with X-ray development (Fuji medical film and Optimax 2010 processor) applied. Untreated cells were used as a negative control and cisplatin-treated (30 μM, 24 h) used as a positive control for the generation of cleaved caspase 3 and γ-H2 AX.

Acknowledgements

A.W. is grateful for a University of Sheffield/A*STARPhD studentship. We also thank the Wellcome Trust for a Postdoctoral Fellowship (M.R.G.) and Dr. D. Robinson for light microscopy support (Wellcome Trust grant: 077544).

Keywords: DNA · imaging · iridium · ruthenium polypyridyl · serum albumin

[1] A. E. Friedman, J. C. Chambron, J. P. Sauvage, N. J. Turro, J. K. Barton, *J. Am. Chem. Soc.* **1990**, *112*, 4960 – 4962.
[2] a) K. E. Erkkila, D. T. Odom, J. K. Barton, *Chem. Rev.* **1999**, *99*, 2777 – 2796; b) C. Metcalfe, J. A. Thomas, *Chem. Soc. Rev.* **2003**, *32*, 215 – 224.
[3] a) B. M. Zeglis, V. C. Pierre, J. K. Barton, *Chem. Commun.* **2007**, 4565 – 4579; b) H. Song, J. T. Kaiser, J. K. Barton, *Nat. Chem.* **2012**, *4*, 615 – 620; c) J. P. Hall, K. O'Sullivan, A. Naseer, J. A. Smith, J. M. Kelly, C. J. Cardin, *Proc. Natl. Acad. Sci. USA* **2011**, *108*, 17610 – 17614; d) H. Niyazi, J. P. Hall, K. O'Sullivan, G. Winter, T. Sorenson, J. M. Kelly, C. J. Cardin, *Nat. Chem.* **2012**, *4*, 621 – 628; e) V. r. C. Pierre, J. T. Kaiser, J. K. Barton, *Proc. Natl. Acad. Sci. USA* **2007**, *104*, 429 – 434; f) Q. Zhao, C. Huang, F. Li, *Chem. Soc. Rev.* **2011**, *40*, 2508 – 2524.
[4] M. R. Gill, J. A. Thomas, *Chem. Soc. Rev.* **2012**, *41*, 3179 – 3192.
[5] A. C. Komor, J. K. Barton, *Chem. Commun.* **2013**, *49*, 3617 – 3630.
[6] a) C. Rajput, R. Rutkaite, L. Swanson, I. Haq, J. A. Thomas, *Chem. Eur. J.* **2006**, *12*, 4611 – 4619; b) M. R. Gill, J. Garcia-Lara, S. J. Foster, C. Smythe, G. Battaglia, J. A. Thomas, *Nat. Chem.* **2009**, *1*, 662 – 667.
[7] a) C. A. Puckett, J. K. Barton, *J. Am. Chem. Soc.* **2007**, *129*, 46 – 47; b) F. R. Svensson, M. Matson, M. Li, P. Lincoln, *Biophys. Chem.* **2010**, *149*, 102 – 106; c) M. R. Gill, D. Cecchin, M. G. Walker, R. S. Mulla, G. Battaglia, C. Smythe, J. A. Thomas, *Chem. Sci.* **2013**, *4*, 4512 – 4519.
[8] a) C. A. Puckett, J. K. Barton, *Bioorg. Med. Chem.* **2010**, *18*, 3564 – 3569; b) L. Cosgrave, M. Devocelle, R. J. Forster, T. E. Keyes, *Chem. Commun.* **2010**, *46*, 103 – 105; c) A. Martin, A. Byrne, C. S. Burke, R. J. Forster, T. E. Keyes, *J. Am. Chem. Soc.* **2014**, *136*, 15300 – 15309.
[9] C. A. Puckett, J. K. Barton, *J. Am. Chem. Soc.* **2009**, *131*, 8738 – 8739.
[10] R. B. P. Elmes, K. N. Orange, S. M. Cloonan, D. C. Williams, T. Gunnlaugsson, *J. Am. Chem. Soc.* **2011**, *133*, 15862 – 15865.
[11] X. Tian, M. R. Gill, I. Cantón, J. A. Thomas, G. Battaglia, *ChemBioChem* **2011**, *12*, 548 – 551.
[12] H. Huang, P. Zhang, B. Yu, Y. Chen, J. Wang, L. Ji, H. Chao, *J. Med. Chem.* **2014**, *57*, 8971 – 8983.
[13] A. Wragg, M. R. Gill, D. Turton, H. Adams, T. M. Roseveare, C. Smythe, X. Su, J. A. Thomas, *Chem. Eur. J.* **2014**, *20*, 14004 – 14011.
[14] J. Bolger, A. Gourdon, E. Ishow, J.-P. Launay, *Inorg. Chem.* **1996**, *35*, 2937 – 2944.
[15] E. Baggaley, M. R. Gill, N. H. Green, D. Turton, I. V. Sazanovich, S. W. Botchway, C. Smythe, J. W. Haycock, J. A. Weinstein, J. A. Thomas, *Angew. Chem. Int. Ed.* **2014**, *53*, 3367 – 3371; *Angew. Chem.* **2014**, *126*, 3435 – 3439.
[16] a) S. Moromizato, Y. Hisamatsu, T. Suzuki, Y. Matsuo, R. Abe, S. Aoki, *Inorg. Chem.* **2012**, *51*, 12697 – 12706; b) R.-R. Ye, C. Tan, L. He, M.-H. Chen, L.-N. Ji, Z.-W. Mao, *Chem. Commun.* **2014**, *50*, 10945 – 10948.
[17] B. A. Albani, B. Peña, N. A. Leed, N. A. B. G. de Paula, C. Pavani, M. S. Baptista, K. R. Dunbar, C. Turro, *J. Am. Chem. Soc.* **2014**, *136*, 17095 – 17101.
[18] D. A. Lutterman, A. Chouai, Y. Liu, Y. Sun, C. D. Stewart, K. R. Dunbar, C. Turro, *J. Am. Chem. Soc.* **2008**, *130*, 1163 – 1170.
[19] J. D. McGhee, P. H. von Hippel, *J. Mol. Biol.* **1974**, *86*, 469 – 489.
[20] L. Lu, H.-Z. He, H.-J. Zhong, L.-J. Liu, D. S.-H. Chan, C.-H. Leung, D.-L. Ma, *Sens. Actuators, B* **2014**, *201*, 177 – 184.
[21] A. R. Timerbaev, C. G. Hartinger, S. S. Aleksenko, B. K. Keppler, *Chem. Rev.* **2006**, *106*, 2224 – 2248.
[22] a) F. Li, Y. Mulyana, M. Feterl, J. M. Warner, J. G. Collins, F. R. Keene, *Dalton Trans.* **2011**, *40*, 5032 – 5038; b) F. Li, M. Feterl, J. M. Warner, A. I. Day, F. R. Keene, J. G. Collins, *Dalton Trans.* **2013**, *42*, 8868 – 8877.
[23] X. M. He, D. C. Carter, *Nature* **1992**, *358*, 209 – 215.
[24] a) D. C. Carter, J. X. Ho, *Adv. Protein Chem.* **1994**, *47*, 153 – 203; b) J. Ghuman, P. A. Zunszain, I. Petitpas, A. A. Bhattacharya, M. Otagiri, S. Curry, *J. Mol. Biol.* **2005**, *353*, 38 – 52.
[25] I. Petitpas, A. A. Bhattacharya, S. Twine, M. East, S. Curry, *J. Biol. Chem.* **2001**, *276*, 22804 – 22809.
[26] H. Mandula, J. M. R. Parepally, R. Feng, Q. R. Smith, *J. Pharmacol. Exp. Ther.* **2006**, *317*, 667 – 675.
[27] O. Mazuryk, K. Magiera, B. Rys, F. Suzenet, C. Kieda, M. Brindell, *J. Biol. Inorg. Chem.* **2014**, *19*, 1305 – 1316.
[28] A. Mazzini, P. Cavatorta, M. Iori, R. Favilla, G. Sartor, *Biophys. Chem.* **1992**, *42*, 101 – 109.
[29] a) M. R. Gill, H. Derrat, C. Smythe, G. Battaglia, J. A. Thomas, *ChemBioChem* **2011**, *12*, 877 – 880; b) A. Wragg, M. R. Gill, C. J. Hill, X. Su, A. J. H. M. Meijer, C. Smythe, J. A. Thomas, *Chem. Commun.* **2014**, *50*, 14494 – 14497.
[30] B. B. Wolf, D. R. Green, *J. Biol. Chem.* **1999**, *274*, 20049 – 20052.
[31] T. Stiff, M. O'Driscoll, N. Rief, K. Iwabuchi, M. Löbrich, P. A. Jeggo, *Cancer Res.* **2004**, *64*, 2390 – 2396.
[32] Z. H. Siddik, *Oncogene* **2003**, *22*, 7265 – 7279.
[33] G. Majno, I. Joris, *Am. J. Pathol.* **1995**, *146*, 3 – 15.
[34] S. M. Vogel, R. D. Minshall, M. Pilipović, C. Tiruppathi, A. B. Malik, *Am. J. Physiol.* **2001**, *281*, L1512 – L1522.
[35] S. Lamansky, P. Djurovich, D. Murphy, F. Abdel-Razzaq, H.-E. Lee, C. Adachi, P. E. Burrows, S. R. Forrest, M. E. Thompson, *J. Am. Chem. Soc.* **2001**, *123*, 4304 – 4312.
[36] J. M. Calvert, J. V. Caspar, R. A. Binstead, T. D. Westmoreland, T. J. Meyer, *J. Am. Chem. Soc.* **1982**, *104*, 6620 – 6627.
[37] N. M. Shavaleev, H. Adams, J. Best, R. Edge, S. Navaratnam, J. A. Weinstein, *Inorg. Chem.* **2006**, *45*, 9410 – 9415.

Received: April 29, 2015
Published online on July 1, 2015